QCD TRANSITION LINE AND CORRELATORS OF CONSERVED CHARGES FROM LATTICE QCD*

Claudia Ratti[a], Rene Bellwied[a], Szabolcs Borsanyi[b]
Zoltan Fodor[c,b,d,e], Jana Guenther[f], Ruben Kara[b]
Sandor Katz[d], Jacquelyn Noronha-Hostler[g], Paolo Parotto[b]
Attila Pasztor[d], Jamie M. Stafford[a], Kalman Szabo[b,e]

[a]Department of Physics, University of Houston, Houston, TX 77204, USA
[b]University of Wuppertal, Department of Physics, 42119 Wuppertal, Germany
[c]Department of Physics, The Pennsylvania State University
University Park, PA 16802, USA
[d]Institute for Theoretical Physics, Eötvös University, 1117 Budapest, Hungary
[e]Jülich Supercomputing Centre, Forschungszentrum Jülich
52428 Jülich, Germany
[f]Aix Marseille Univ., Université de Toulon, CNRS, CPT, Marseille, France
[g]Illinois Center for Advanced Studies of the Universe, Department of Physics
University of Illinois at Urbana-Champaign, Urbana, IL 61801, USA

We review recent results on the QCD phase transition line and second-order fluctuations and correlators of conserved charges calculated in lattice QCD. In the case of fluctuations, we compare them to the Hadron Resonance Gas model and construct proxies that allow a direct comparison between first principle simulations and measurements.

1. Introduction

We live in a very exciting era for the study of strongly interacting matter under extreme condition. The experimental program at RHIC is running till 2021 with the Second Beam Energy Scan (BESII), trying to find the elusive critical point on the phase diagram of strongly interacting matter. The study of dense matter will not finish with RHIC, as the FAIR facility with its Compressed Baryonic Matter (CBM) program is currently being built

---

* Presented at the on-line meeting *Criticality in QCD and the Hadron Resonance Gas*, Wrocław, Poland, July 29–31, 2020.

at the GSI in Germany and the NICA program will start running in a few years. Besides, new exciting possibilities to study the properties of ultra-dense matter are coming from astrophysical observations of Gravitational Wave and Neutron Star properties.

Lattice QCD can provide results for several first principle observables to support the experimental program, such as the equation of state, which is needed as an input in hydrodynamical simulations, the QCD transition line and constraints on the location of the critical point, and fluctuations of conserved charges. At the moment, direct simulations at finite chemical potential μ_B are not possible due to the sign problem. There are two main alternative methods to extend the lattice results to finite density: the Taylor expansion of thermodynamic observables in powers of μ_B/T [1–13] or simulations at imaginary μ_B, followed by an analytical continuation of the results to real μ_B [14–31].

In this contribution, we will focus on the latter, discussing the recent results from our collaboration on the phase transition line [32] and correlators of conserved charges [33], and proposing measurements that can be compared to our data.

2. The phase transition line

The QCD transition line can be parametrized as follows:

$$\frac{T_c(\mu_B)}{T_c(\mu_B = 0)} = 1 - \kappa_2 \left(\frac{\mu_B}{T_c(\mu_B)} \right)^2 - \kappa_4 \left(\frac{\mu_B}{T_c(\mu_B)} \right)^4 + \dots, \qquad (1)$$

which we will calculate along the strangeness neutrality line, a trajectory in the QCD phase diagram which is relevant to phenomenology, as the values of μ_S and μ_Q (strangeness and electric charge chemical potentials) are functions of T and μ_B that satisfy the following experimental conditions:

$$\langle n_S \rangle = 0, \qquad \langle n_Q \rangle = 0.4 \langle n_B \rangle. \qquad (2)$$

The coefficients κ_2 and κ_4 can be determined by either one of the standard extrapolation methods listed above. A direct evaluation of the μ_B-derivatives at $\mu_B = 0$ was used in Refs. [10, 34, 35]. Here, we use the analytical continuation from imaginary-μ_B method, which results in a larger signal-to-noise ratio [23, 24]. The results for κ_2 obtained with the two methods were thoroughly compared in Ref. [29].

The observables under study are the renormalized dimensionless chiral condensate and susceptibility, defined as

$$\langle \bar{\psi}\psi \rangle = - \left[\langle \bar{\psi}\psi \rangle_T - \langle \bar{\psi}\psi \rangle_0 \right] \frac{m_{ud}}{f_\pi^4}, \qquad (3)$$

$$\chi = [\chi_T - \chi_0] \frac{m_{ud}^2}{f_\pi^4}, \qquad \text{with} \qquad (4)$$

$$\langle \bar{\psi}\psi \rangle_{T,0} = \frac{T}{V} \frac{\partial \log Z}{\partial m_{ud}}, \qquad \chi_{T,0} = \frac{T}{V} \frac{\partial^2 \log Z}{\partial m_{ud}^2}, \qquad (5)$$

where $m_u = m_d = m_{ud}$. The subscripts $T, 0$ indicate values at finite- and zero-temperature, respectively. In the following, $\langle \bar{\psi}\psi \rangle$ (the chiral condensate) and χ (the chiral susceptibility) are always shown after applying the correction to satisfy $\langle n_s \rangle = 0$ with zero statistical error.

Our results are obtained using 4-stout improved staggered fermions with an aspect ratio $LT = 4$ and temporal lattice sizes $N_t = 10, 12, 16$. The quark masses are set at their physical values. The upper left and right panels of Fig. 1 show the chiral condensate and susceptibility as functions of the
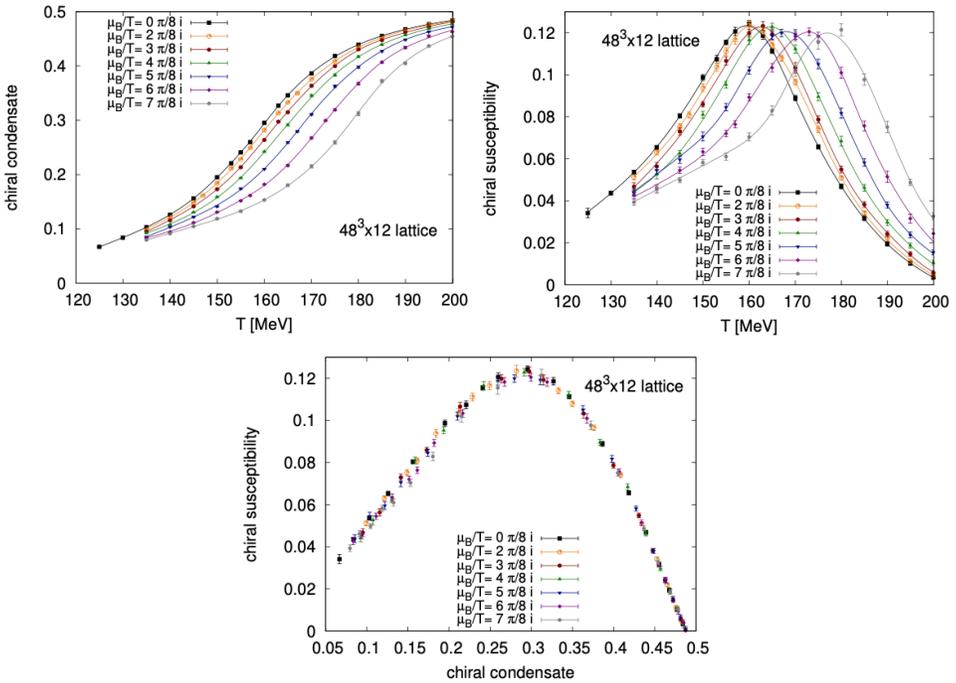
Fig. 1. (Color online) Renormalized chiral condensate $\langle \bar{\psi}\psi \rangle$ (upper left) and chiral susceptibility χ (upper right) as functions of the temperature for the intermediate lattice spacing in this study. The black, first from the top, curves correspond to vanishing baryon density, while results for various imaginary values of the chemical potential are shown in shades of grey (other colors). Finally, in the lower panel, we show the susceptibility as a function of the condensate. In this representation, the chemical potential dependence is very weak.

temperature, calculated at different values of the imaginary chemical potential. The lower panel shows the chiral susceptibility plotted as a function of the chiral condensate. It is clear from this last plot that the chemical potential dependence of the curves is lost in this case. We exploit this feature in our analysis, which leads to a more precise determination of T_c and, as a consequence, of κ_2 and κ_4. In fact, it allows a simple parametrization of χ as a function of $\langle \bar{\psi}\psi \rangle$ in terms of a low-order polynomial. The peak in $\langle \bar{\psi}\psi \rangle$ corresponds to a "critical value" of $\langle \bar{\psi}\psi \rangle$, which in turn identifies a value for the transition temperature. The uncertainty in several of the steps described above leads to 256 independent analysis, which are folded into the systematic error. Our results are

$$
\begin{aligned}
T_c &= 158.0 \pm 0.6 \text{ MeV} , \\
\kappa_2 &= 0.0153 \pm 0.0018 , \\
\kappa_4 &= 0.00032 \pm 0.00067 .
\end{aligned}
\tag{6}
$$

We show the corresponding transition line in the left panel of Fig. 2. We introduce a width parameter σ, which corresponds to the half width of the transition

$$
\langle \bar{\psi}\psi \rangle (T_c \pm \sigma/2) = \langle \bar{\psi}\psi \rangle_c \pm \Delta \langle \bar{\psi}\psi \rangle /2 ,
\tag{7}
$$

with $\langle \bar{\psi}\psi \rangle_c = 0.285$ and $\Delta \langle \bar{\psi}\psi \rangle = 0.14$. We show σ in the right panel of Fig. 2. It turns out that the half width is consistent with a constant
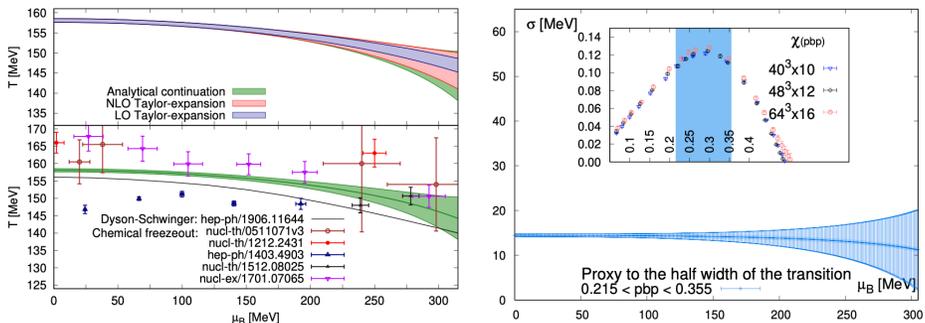
Fig. 2. (Color online) Left: Top — Transition line extrapolated from lattice simulations at imaginary chemical potential (gray/green band) compared with an extrapolation using the formula in Eq. (1) up to κ_4 (light gray/red band) or up to κ_2 (dark gray/blue band). Bottom — Our crossover transition line compared to a prediction from truncated Dyson–Schwinger equations [36] and some estimates of the chemical freezeout parameters in heavy-ion collisions [37–41]. Right: Half width of the transition. In the inset we show a plot of the $\chi(\langle \bar{\psi}\psi \rangle)$ peak, where the shaded region corresponds to $\langle \bar{\psi}\psi \rangle_c \pm \Delta \langle \bar{\psi}\psi \rangle /2$. Both are extrapolated to real μ_B.

for $\mu_B \approx 300$ MeV. Since the width is supposed to become narrow when a critical point is approached, we conclude that our results do not exhibit any sign of criticality in the explored μ_B range.

3. Cross-correlators of conserved charges

Given the ongoing measurements of correlators between different particles by the STAR Collaboration [42], we want to build a bridge between the correlators of conserved charges from lattice QCD and the experimental measurements of correlations and fluctuations of hadronic species, in particular for the correlator of baryon number and strangeness. The Hadron Resonance Gas (HRG) model is used for this purpose, as it allows us to isolate correlations between single particles and connect them to correlators of conserved charges.

Fluctuations of conserved charges are expressed as derivatives of the grand partition function with respect to the different chemical potentials. In the HRG model, they can be written as

$$\chi_{ijk}^{BQS}(T, \hat{\mu}_B, \hat{\mu}_Q, \hat{\mu}_S) = \frac{\partial^{i+j+k}\left(p/T^4\right)}{\partial\hat{\mu}_B^i \partial\hat{\mu}_Q^j \partial\hat{\mu}_S^k} = \sum_R B_R^i\, Q_R^j\, S_R^k\, I_{i+j+k}^R(T, \hat{\mu}_B, \hat{\mu}_Q, \hat{\mu}_S)\,,$$

(8)

where $\hat{\mu}_i = \mu_i/T$, and I_{i+j+k}^R reads (note that it is completely symmetric in all indices, hence $i + j + k = l$)

$$I_l^R(T, \hat{\mu}_B, \hat{\mu}_Q, \hat{\mu}_S) = \frac{\partial^l p_R/T^4}{\partial\hat{\mu}_R^l}\,,$$

(9)

where $\mu_R = \mu_B B_R + \mu_Q Q_R + \mu_S S_R$. We can replace the sum in Eq. (8) as a sum over the stable states under strong interactions

$$\sum_R B_R^l Q_R^m S_R^n I_p^R \rightarrow \sum_{i \in \text{stable}} \sum_R (P_{R \rightarrow i})^p\, B_i^l Q_i^m S_i^n I_p^R\,,$$

(10)

where $(P_{R \rightarrow i})^p$ is the average number of particles i obtained from the decay of particle R.

By writing the fluctuations in Eq. (8) in term of stable particles, we can distinguish between particles which can be detected in experiment and those which usually are not. In this work, we employ the hadronic list labeled PDG2016+ in [27], with the list of decays described and first utilized in [43]. We will label the following species 'measured'

$$\pi^\pm\,, \quad K^\pm\,, \quad p\,(\bar{p})\,, \quad \Lambda\,(\bar{\Lambda})\,, \quad \Xi^-\,(\bar{\Xi}^+)\,, \quad \Omega^-\,(\bar{\Omega}^+)\,,$$

where we note that, since the decay $\Omega^0 \rightarrow \Lambda + \gamma$ has a branching ratio of $\sim 100\%$, what we indicate as Λ also contains the entire Ω^0 contribution.

In the left panel of Fig. 3, we show the lattice QCD results for the χ_{11}^{BS} correlator as a function of the temperature at $\mu_B = 0$ at different finite spacings, as well as its continuum extrapolation. In the right panel, we compare this continuum extrapolation to the results from our HRG model analysis, where we separate the contribution from measured and non-measured hadronic species. We notice that the contributions roughly correspond to the same amount. In Fig. 4, we show the breakdown of the main contributions from measured particles to $-\chi_{11}^{BS}$ and χ_2^S at $\mu_B = 0$.
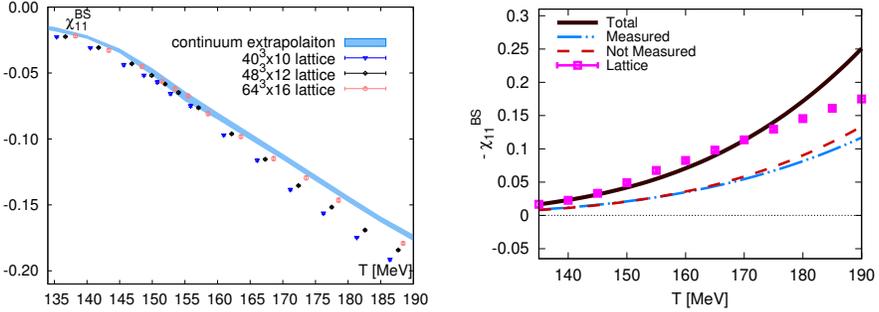
Fig. 3. (Color online) From Ref. [33]. Left: Continuum extrapolated results for the correlator χ_{11}^{BS} as a function of the temperature at $\mu_B = 0$ (gray/blue band). The different datapoints correspond to results at finite lattice spacing. Right: Lattice results compared to HRG model calculations (solid black line), with the contribution from measured (dot-dashed blue line) and non-measured (dashed red line) hadronic species.
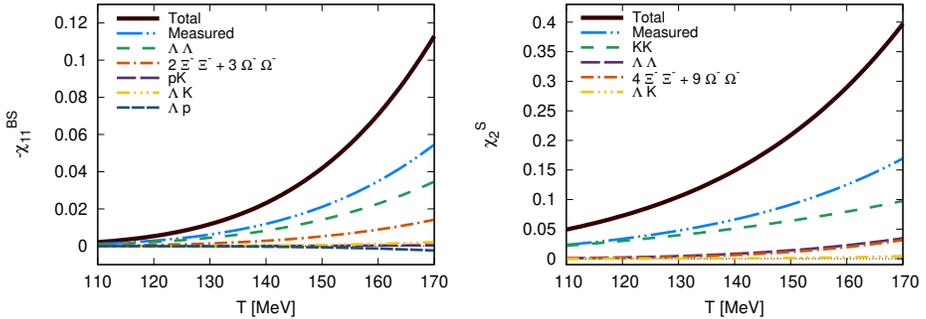
Fig. 4. From Ref. [33]. Contributions from 'measured' states to $-\chi_{11}^{BS}$ (left panel) and χ_2^S (right panel), at $\mu_B = 0$, as functions of the temperature.

To perform a comparison to experiment and to lattice QCD results, exploiting the information in Fig. 4, we construct the following proxy for the ratio $-\chi_{11}^{BS}/\chi_2^S$:

$$\widetilde{C}_{BS,SS}^{\Lambda,\Lambda K} = \sigma_\Lambda^2 / \left(\sigma_K^2 + \sigma_\Lambda^2 \right) , \tag{11}$$

which is shown in the left panel of Fig. 5 as a dotted blue line, together with the full HRG result (solid black line). This quantity reproduces the full result for all temperatures around the QCD transition. The right panel shows a comparison of this proxy, calculated along parametrized freeze-out lines with $T(\mu_B = 0) = 145, 165$ MeV, to preliminary STAR data. We notice that the data prefer the higher freeze-out temperature. This is in agreement with previous findings [39, 44–47].
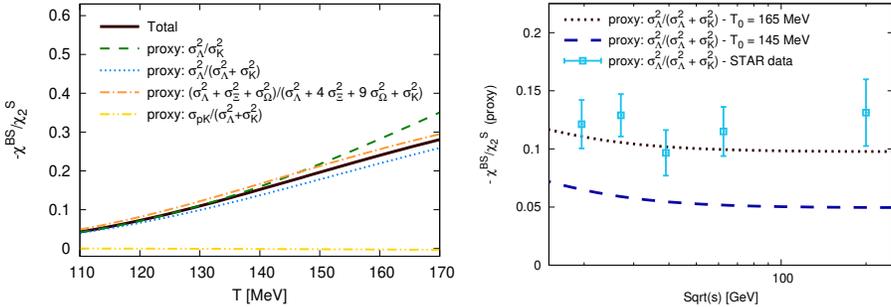
Fig. 5. (Color online) From Ref. [33]. Left: Comparison of different proxies (the dotted blue line shows $\widetilde{C}_{BS,SS}^{\Lambda,\Lambda K}$) and the total result (solid black line) for $-\chi_{11}^{BS}/\chi_2^S$ at $\mu_B = 0$. Right: Comparison of our proxy with the kinematic cuts from [48, 49], along parametrized freeze-out lines with $T(\mu_B = 0) = 145, 165$ MeV (dotted black and dashed blue). The light blue dots show STAR preliminary data.

4. Conclusions

We presented our most recent results on the transition line of QCD and on correlators of conserved charges. In particular, we focused on the correlator between baryon number and strangeness. We found a proxy which reproduces the lattice QCD results at all explored temperatures and chemical potentials. We then compared the HRG model predictions for the proxy to the corresponding experimental results and found that they can be reproduced with a freeze-out temperature which is in agreement with previous results for strange fluctuations.

REFERENCES

[1] C. Allton *et al.*, *Phys. Rev. D* **66**, 074507 (2002).

[2] C. Allton *et al.*, *Phys. Rev. D* **71**, 054508 (2005).

[3] R. Gavai, S. Gupta, *Phys. Rev. D* **78**, 114503 (2008).

[4] MILC Collaboration (S. Basak *et al.*), *PoS* **LATTICE2008**, 171 (2008).

[5] S. Borsányi *et al.*, *J. High Energy Phys.* **1201**, 138 (2012).

[6] S. Borsányi *et al.*, *J. High Energy Phys.* **1208**, 053 (2012).

[7] R. Bellwied *et al.*, *Phys. Rev. D* **92**, 114505 (2015).

[8] H.-T. Ding *et al.*, *Phys. Rev. D* **92**, 074043 (2015).

[9] A. Bazavov *et al.*, *Phys. Rev. D* **95**, 054504 (2017).

[10] HotQCD Collaboration (A. Bazavov *et al.*), *Phys. Lett. B* **795**, 15 (2019).

[11] A. Bazavov *et al.*, *Phys. Rev. D* **101**, 074502 (2020).

[12] M. Giordano, A. Pásztor, *Phys. Rev. D* **99**, 114510 (2019).

[13] M. Giordano *et al.*, *Phys. Rev. D* **101**, 074511 (2020).

[14] Z. Fodor, S. Katz, *Phys. Lett. B* **534**, 87 (2002).

[15] Z. Fodor, S. Katz, *J. High Energy Phys.* **0203**, 014 (2002).

[16] P. de Forcrand, O. Philipsen, *Nucl. Phys. B* **642**, 290 (2002).

[17] M. D'Elia, M.P. Lombardo, *Phys. Rev. D* **67**, 014505 (2003).

[18] Z. Fodor, S. Katz, *J. High Energy Phys.* **0404**, 050 (2004).

[19] M. D'Elia, F. Sanfilippo, *Phys. Rev. D* **80**, 014502 (2009).

[20] P. Cea, L. Cosmai, A. Papa, *Phys. Rev. D* **89**, 074512 (2014).

[21] C. Bonati *et al.*, *Phys. Rev. D* **90**, 074030 (2014).

[22] P. Cea, L. Cosmai, A. Papa, *Phys. Rev. D* **93**, 014507 (2016).

[23] C. Bonati *et al.*, *Phys. Rev. D* **92**, 054503 (2015).

[24] R. Bellwied *et al.*, *Phys. Lett. B* **751**, 559 (2015).

[25] M. D'Elia, G. Gagliardi, F. Sanfilippo, *Phys. Rev. D* **95**, 094503 (2017).

[26] J. Guenther *et al.*, *Nucl. Phys. A* **967**, 720 (2017).

[27] P. Alba *et al.*, *Phys. Rev. D* **96**, 034517 (2017).

[28] V. Vovchenko *et al.*, *Phys. Lett. B* **775**, 71 (2017).

[29] C. Bonati *et al.*, *Phys. Rev. D* **98**, 054510 (2018).

[30] S. Borsanyi *et al.*, *J. High Energy Phys.* **1810**, 205 (2018).

[31] A. Pásztor, Z. Szép, G. Markó, arXiv:2010.00394 [hep-lat].

[32] S. Borsanyi *et al.*, *Phys. Rev. Lett.* **125**, 052001 (2020).

[33] R. Bellwied *et al.*, *Phys. Rev. D* **101**, 034506 (2020).

[34] O. Kaczmarek *et al.*, *Phys. Rev. D* **83**, 014504 (2011).

[35] G. Endrődi, Z. Fodor, S. Katz, K. Szabó, *J. High Energy Phys.* **1104**, 001 (2011).

[36] P. Isserstedt, M. Buballa, C.S. Fischer, P.J. Gunkel, *Phys. Rev. D* **100**, 074011 (2019).

[37] A. Andronic, P. Braun-Munzinger, J. Stachel, *Nucl. Phys. A* **772**, 167 (2006).

[38] F. Becattini *et al.*, *Phys. Rev. Lett.* **111**, 082302 (2013).

[39] P. Alba *et al.*, *Phys. Lett. B* **738**, 305 (2014).

[40] V. Vovchenko, V. Begun, M. Gorenstein, *Phys. Rev. C* **93**, 064906 (2016).

[41] STAR Collaboration (L. Adamczyk *et al.*), *Phys. Rev. C* **96**, 044904 (2017).

[42] STAR Collaboration (J. Adam *et al.*), *Phys. Rev. C* **100**, 014902 (2019).

[43] P. Alba *et al.*, *Phys. Rev. C* **98**, 034909 (2018).

[44] P. Alba *et al.*, *Phys. Rev. C* **101**, 054905 (2020).

[45] R. Bellwied *et al.*, *Phys. Rev. C* **99**, 034912 (2019).

[46] J. Noronha-Hostler *et al.*, arXiv:1607.02527 [hep-ph].

[47] R. Bellwied *et al.*, *Phys. Rev. Lett.* **111**, 202302 (2013).

[48] STAR Collaboration (L. Adamczyk *et al.*), *Phys. Lett. B* **785**, 551 (2018).

[49] STAR Collaboration (T. Nonaka), *Nucl. Phys. A* **982**, 863 (2019).